Self-assembled "Supra-molecular" Structures via Hydrogen Bonding and Aromatic/Aliphatic Microphase Separation on Different Length Scales in Symmetric-Tapered Bisamides

ARTICLE *in* CHEMISTRY OF MATERIALS · FEBRUARY 2004

Impact Factor: 8.35 · DOI: 10.1021/cm0349755

Self-assembled "Supra-molecular" Structures via Hydrogen Bonding and Aromatic/Aliphatic Microphase Separation on Different Length Scales in Symmetric-Tapered Bisamides

Chenchen Xue, Shi Jin,* Xing Weng, Jason J. Ge, Zhihao Shen, Hong Shen, Matthew J. Graham, Kwang-Un Jeong, Huabing Huang, Dong Zhang, Mingming Guo, Frank W. Harris, and Stephen Z. D. Cheng*

Maurice Morton Institute and Department of Polymer Science, The University of Akron, Akron, Ohio 44325-3909

Christopher Y. Li

Department of Materials Science and Engineering, Drexel University, Philadelphia, Pennsylvania 19104

Lei Zhu

Polymer Program, Institute of Materials Science and Department of Chemical Engineering, The University of Connecticut, Storrs, Connecticut 06269-3136

Received October 8, 2003. Revised Manuscript Received January 11, 2004

Self-assembled "supra-molecular" liquid-crystalline phases were investigated in one of a series of symmetrically tapered bisamides based on an amide core of 1,2-bis[3,4,5-tris(alkan-1-yloxy)benzamido]benzene and three alkyl tails on each side of the core. One of this series of bisamides having 14 carbon atoms in each tail (abbreviated as C_{14}PhBA) served as an example in this study. Differential scanning calorimetry thermal diagrams showed two main phase transition processes in C_{14}PhBA. Wide-angle X-ray diffraction results revealed that the high-temperature phase transition is between the isotropic melt (I) and a 2D low-ordered oblique columnar phase (I ↔ Φ_{OB}). The low-temperature phase transition was attributed to the transition between a highly ordered, oblique columnar (Φ_{OK}) phase and the Φ_{OB} phase. Supra-molecular columns were directly visualized using transmission electron microscopy and atomic force microscopy. The formation of these supra-molecular structures is critically dependent upon the construction of building blocks ("columns") by C_{14}PhBA molecules. These building blocks developed via rigid amide core/alkyl tail micro-phase separation and the hydrogen (H) bond formation between the N−H and carbonyl groups among the cores. Spectroscopic studies showed that the columns were stabilized by intercore H-bonds oriented along the column long axis, and the alkyl tails in the Φ_{OK} phase were packed into an ordered mesophase having about 64% of the methylene carbon atoms in long trans segments at room temperature. In the Φ_{OB} phase, the alkyl tails adopt liquidlike disordered conformations. The high- and low-temperature phase transitions were thus mainly attributed to the sudden changes in H-bonding and alkyl tail conformation, respectively. A detailed packing model of the Φ_{OK} phase was proposed and qualitatively proven using a simulated structural diffraction.

Introduction

The concept of self-assembling "supra-molecular" architecture has been defined as chemistry beyond molecules. It involves investigating new systems in which intermolecular physical interactions are used to construct building blocks and hold these blocks together rather than using covalent bonds. A number of noncovalent interactions have been found to be responsible in the formation of supra-molecular systems. They include hydrogen (H) bonding, electrostatic (ion−ion, ion−dipole, and dipole−dipole) interactions, $\pi-\pi$ stacking interactions, van der Waals interactions, and hydrophobic−hydrophilic effects along with others. Among these interactions, H-bonding has become a topic of major research due to its numerous potential applications in the biological and material sciences.[1−5] For example, tubular structures based on self-assembling

* Authors to whom correspondence should be addressed. E-mail: scheng@uakron.edu.

(1) Eisenberg, B. *Acc. Chem. Res.* **1998**, *31*, 117−123.
(2) Lehn, J.-M. *Angew. Chem.* **1988**, *100*, 91−116.
(3) Lehn, J.-M. *Angew. Chem., Int. Ed. Engl.* **1990**, *29*, 1304−1319.
(4) Whitesides, G. M.; Mathias, J. P.; Seto, C. T. *Science* **1991**, *254*, 1312−1319.
(5) Schneider, H. J., Durr, H., Eds. *Frontiers in Supramolecular Organic Chemistry and Photochemistry*; VCH: New York, 1991.

10.1021/cm0349755 CCC: $27.50
Published on Web 02/20/2004

ring-shaped peptides by "inter-rings" of H-bonds were reported to be developed for trans-membrane ion channels,[6,7] biosensors,[8] and potential novel drug delivery vehicles.[9−11] Inspired by the bilayer fluid mosaic of the cell membrane structure modeled in nature, wedge-shaped trialkylated phenoxy sectors can be assembled into supra-molecular disks that subsequently stack to form a continuous liquid-crystalline (LC) columnar phase.[12−15] Therefore, because of their directionality and versatility, H-bonding holds the most powerful organizing force to construct self-assemblies utilizing the donor−acceptor approach in natural amides.[16−18]

In addition to H-bonding, the demixing of a two-component system represents a classical pathway to facilitate phase separation on different length scales due to the incompatibility of the two components. Great efforts have been made to learn how to control the morphology of self-assembled, micro-phase separation in traditional immiscible polymer blends which are usually affected by factors associated with the thermodynamics and kinetics of phase separation. In molecules that include both rigid aromatic cores and flexible segments, the rigid and flexible parts are microscopically separated, yet they are covalently connected. This micro-phase separation leads to a controlled self-assembly process.

In recent years, researchers have been designing molecules as building blocks by combining both H-bonding and micro-phase separation. One of these approaches has been the design of single- or twin-tapered molecules. A typical single-tapered molecule design is asymmetric and includes a rigid core with several aliphatic chains attached at one end of the core. At the other end, H-bonding groups are usually available to make sure that the micro-phase separation leads to the aliphatic chains pointing outward and the rigid cores are connected by H-bonding at the center.[19−21] Each single-tapered molecule becomes a building block to form a part of the disk. It often occupies one-third to one-sixth of a disk and, thus, three to six molecules form one disk, and those disks then stack together to generate a column.

For the designs of twin-tapered molecules, which are chemically symmetric, a rigid core is at the center and the two ends of the rigid core link alkyl tails. The rigid core can be a single peptide or benzamide group. These tails are usually alkyl chains with several to over 10 carbon atoms. The existence of these alkyl tails induces the micro-phase separation. This type of molecule apparently does not have the ability to assemble into a columnar structure. However, a different conclusion may be reached if both the steric hindrance and H-bonding were put into consideration. In this type of system, H-bonds are almost exclusively formed between N−H and C═O groups, and preferably from two neighboring cores. One possible way to form these H-bonds is to make sheetlike stacks. However, this stacking generates a tremendous steric hindrance caused by the multiple alkyl tails. To release steric hindrance, molecules may adopt another possible arrangement in which neighboring molecules stack perpendicular to each other.[22] If the latter case is preferred, columns can be constructed and the direction of the H-bonds are parallel to the long axis of the column. Although this potential model was deduced by the observed columnar structure using X-ray diffraction experiments, a detailed stacking model has not been presented.

Recently, a series of bisamide molecules were synthesized which contain 1,2-bis[3,4,5-tris (alkan-1-yloxy)-benzamido]benzene as a rigid core with three alkyl tails at each end of the core. The rigid core has a rigid plane with a configuration of three phenylenes linked by two amide groups. In this study, the molecule with 14 carbons tails (C_{14}PhBA) is used as a representative of the series. On the basis of our experimental observations about the phase transition thermodynamic properties, phase structure identifications, phase structure evolutions, H-bonding orientation, and alkyl tail conformations, we can conclude that micro-phase separation of the rigid cores and alkyl tails and H-bond formation among the rigid cores construct stable columns to form columnar phases. Furthermore, the lateral packing of the columns depends on the organization of the alkyl tails. The disordered, liquidlike alkyl tails are compatible with the low-ordered Φ (Φ_{OB}) phase, while the ordered alkyl tails exist in the highly ordered Φ (Φ_{OK}) phase.

Experimental Section

Materials Synthesis and Sample Preparations. A series of symmetric-tapered bisamides were synthesized, and the one with 14 carbons in each alkyl tail was chosen for this study. The synthetic route is shown in Scheme 1. In this case, n = 14. The sample was purified by chromatography on silica gel using acetone−benzene (0.05/0.95) mixed solvents as eluent. The samples were then vacuum-dried. The purity of the samples was verified by thin-layer chromatography and nuclear magnetic resonance.

The sample was kept in a vacuum before carrying out characterization and analysis. For differential scanning calorimetry (DSC) experiments, the sample weight was about 2.0 mg and the pan weights were kept constant with a precision

(6) Seebach, D.; Matthews, J. L.; Meden, A.; Wessels, T.; Baerlocher, C.; McCusker, L. B. *Helv. Chim. Acta* **1997**, *80*, 173−182.
(7) Ranganathan, D.; Lakshmi, C.; Karle, I. L. *J. Am. Chem. Soc.* **1999**, *121*, 6103−6107.
(8) Motesharei, K.; Ghadiri, M. R. *J. Am. Chem. Soc.* **1997**, *119*, 11306−11312 and references therein.
(9) Harada, A.; Li, J.; Kamachi, M. *Nature* **1993**, *364*, 516−518.
(10) Schnur, J. M. *Science* **1993**, *262*, 1669−1676.
(11) Hartgerink, J. D.; Granja, J. R.; Milligan, R. A.; Ghadiri, M. R. *J. Am. Chem. Soc.* **1996**, *118*, 43−50.
(12) Percec, V.; Schlueter, D.; Ungar, G.; Cheng, S. Z. D.; Zhang, A. *Macromolecules* **1998**, *31*, 1745−1762.
(13) Percec, V.; Ahn, C.-H.; Cho, W.-D.; Jamieson, A. M.; Kim, J.; Leman, T.; Schmidt, M.; Gerle, M.; Möller, M.; Prokhorova, S. A.; Sheiko, S. S.; Cheng, S. Z. D.; Zhang, A.; Ungar, G.; Yeardley, D. J. P. *J. Am. Chem. Soc.* **1998**, *120*, 8619−8631.
(14) Percec, V.; Bera, T. K. *Biomacromolecules* **2002**, *3*, 167−181 and references therein.
(15) Raïs, K.; Daoud, M.; Gharbia, M.; Gharbi, A.; Nguyen, H. T. *Chemphyschem* **2001**, *1*, 45.
(16) Krische, M. J.; Lehan, J. -M. *Struct. Bonding (Berlin)* **2000**, *96*, 3−29.
(17) Sijbesma, R. P.; Meijer, E. W. *Curr. Opin. Colloid Interface Sci.* **1999**, *4*, 24−32.
(18) Fredericks, J. R.; Hamilton, A. D. *Comprehensive Supramolecular Chemistry*; Lehan, J.-M., Ed.; Pergamon: New York, 1996; Chapter 16.
(19) Ciuchi, F.; Nicola, G. D.; Franz, H.; Gottarelli, G.; Mariani, P.; Bossi, M. G. P.; Spada, G. P. *J. Am. Chem. Soc.* **1994**, *116*, 7064−7071.
(20) Kleppinger, R.; Lillya, C. P.; Yang, C. *J. Am. Chem. Soc.* **1997**, *119*, 4097−4102.
(21) Suarez, M.; Lehn, J.-M.; Zimmerman, S. C.; Skoulios. A.; Heinrich, B. *J. Am. Chem. Soc.* **1998**, *120*, 9526−9532.
(22) Ungar, G.; Abramic, D.; Percec, V.; Heck, J. A. *Liq. Cryst.* **1996**, *21*, 73−86.

Scheme 1. Synthetic Route of 1,2-Bis[3,4,5-tris(alkan-1-yloxy)benzamido]benzenes

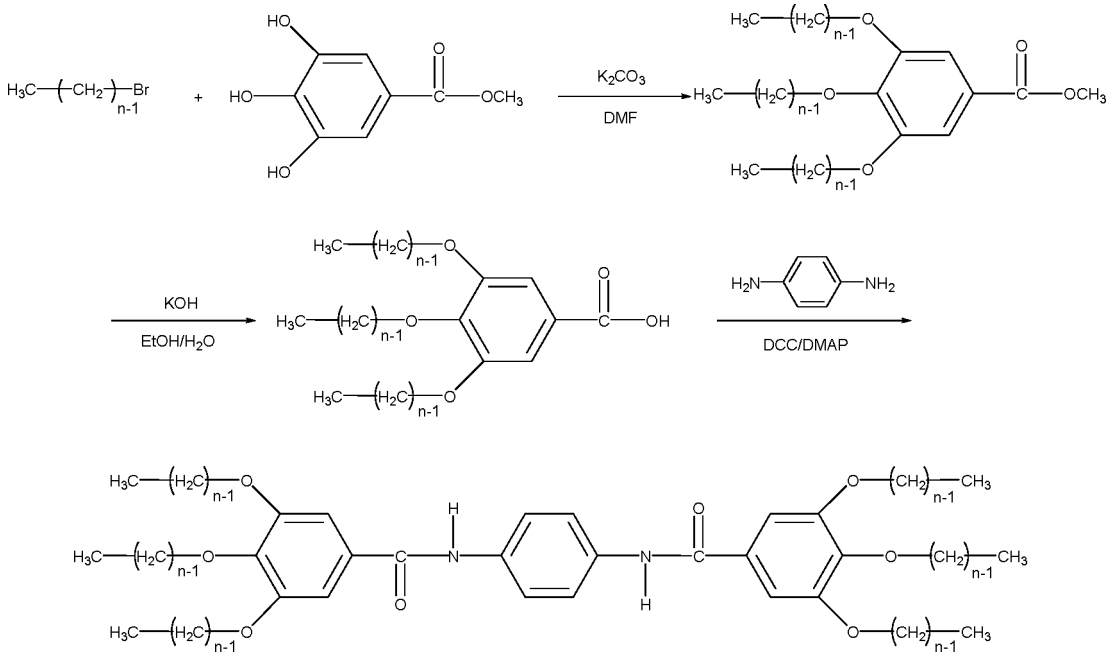

of ±0.001 mg. To observe the evolution of different phase structures, C_{14}PhBA films (0.5 mm) were prepared in the melt for one-dimensional (1D) wide-angle X-ray diffraction (WAXD) powder experiments. The oriented samples for 2D WAXD experiments were made by mechanically shearing the sample at 100 °C. To prepare transmission electron microscopy (TEM), atomic force microscopy (AFM) samples, a dilute solution (0.001−0.005% in $CHCl_3$) was used and cast on carbon-coated glass substrates. The samples were heated on a hot stage (Mettler FP-90) to above the isotropization temperature (160 °C) in a dry nitrogen atmosphere to remove the solvent. They were then subsequently cooled to room temperature, and thin films with a thickness of 30−100 nm were obtained.

Equipment and Experiments. DSC experiments were performed on a Perkin-Elmer PYRIS Diamond DSC. The temperature and heat flow scales were calibrated using standard materials at different cooling and heating rates (between 2.5 and 20 °C/min). Transition temperatures were determined using the onset temperatures. An onset temperature was defined by the cross-point of the peak slope and the baseline in the DSC trace. In cooling, the onset temperature was determined on the high-temperature side, and upon heating the onset temperature determined was on the low-temperature side.

Phase structures and transformations were identified using 1D WAXD experiments. These were carried out using a diffractometer on a Rigaku 12-kW rotating-anode generator (Cu Kα) coupled with a hot stage. For the time-resolved heating and cooling experiments, the 2θ in the refection mode had a scanning rate of 7°/min. To identify different phase structures, 2D WAXD fiber experiments were conducted on a Rigaku 18-kW rotating-anode generator (Cu Kα) equipped with an image plate and a hot stage. High-quality fiber patterns were obtained after one-half to 1-h exposure times. Both X-ray beams were monochromatized using graphite crystals. The diffraction 2θ positions and widths observed on the powder and fiber patterns were calibrated with silicon crystals with known 2θ diffractions and crystallite sizes when $2\theta > 15°$ and calibrated with silver behenate when $2\theta < 15°$. The deviation of the measured diffraction angle was ±0.05°. The crystal unit-cell determination procedure was based on construction of the reciprocal lattice. Computer refinements were conducted to find the solutions with the least error between calculated values and experimental results.[23]

H-bonding and molecular conformations were studied using variable-temperature FT-IR with a DigiLab FTS-3000 spectrometer equipped with a hot stage and was purged by nitrogen. An approximately 1.5-mg sample was sandwiched between two KBr windows. The sample was first heated to the I state and then cooled to room temperature to eliminate previous thermal history. The temperature was held constant when a spectrum was being acquired. The heating rate between temperatures was 2.5 °C/min and each temperature was held for at least 5 min before a measurement to ensure temperature equilibration. The resolution was 1 cm^{-1} and 40 scans were co-added for each spectrum. Raman measurements were carried out on a Bruker RFS-100 FT-Raman spectrometer using a 1.064-μm excitation. The laser power was 200 mW. The resolution was 2 cm^{-1} and 200 scans were collected. The thermal treatment was the same as used in FT-IR experiments. Polarized IR spectroscopy experiments were carried out on a Mattson Galaxy Series FT-IR 5000 with a polarizer. The resolution was 4 cm^{-1}. A dichroic ratio ($A_{//}/A_{\perp}$) was calculated as the ratio of intensities from the corresponding absorption peak from the spectrum with infrared beam's polarization direction parallel (0°) and perpendicular (90°) to the orientation direction.

Solid state ^{13}C NMR experiments were conducted on a Chemagnetics CMX 200 spectrometer operating at 201.13 and 50.78 MHz for ^{1}H and ^{13}C nuclei, respectively. The samples were spun in nitrogen gas at 4.5 kHz at the magic angle. The ^{13}C CP/MAS/DD NMR spectra were acquired over a temperature range between room temperature and 168 °C, which is higher than the highest transition temperature in C_{14}PhBA. The proton decoupling field was of the same strength as the spin-lock field. The magic angle was optimized by the intensity calibration of the aromatic carbon resonance of hexamethyl benzene. The contact time was 1 ms. The Bloch decay spectra with MAS were conducted to selectively study the mobile components. ^{13}C NMR spectra were recorded from an isothermal state after a preset temperature was reached and held for 30 min. Each spectrum consists of an accumulation of 300 scans. The proton 90°-pulse width was set at 4.3 μs for ^{13}C and the recycle delay between the successive pulse sequences was 5 s. Gated high-power proton decoupling at 63 kHz was used to avoid the nuclear Overhauser effect.

Morphological observation of LC phases on the micrometer scale was conducted on an Olympus (HB-2) PLM coupled with

(23) Eashoo, M.; Wu, Z.; Zhang, A.; Shen, D.; Tse, C.; Harris, F. W.; Cheng, S. Z. D.; Gardner, K. H.; Hsiao, B. S. *Macromol. Chem. Phys.* **1994**, *195*, 2207−2225.

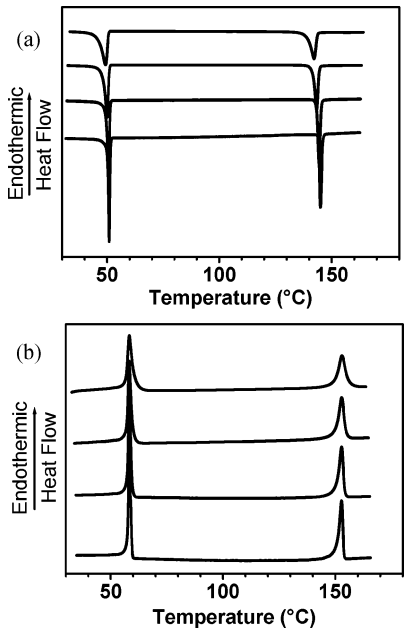

Figure 1. Two sets of DSC diagrams for C_{14}PhBA (a) during cooling (cooling rates from the top trace to the bottom trace: 20, 10, 5, 2.5 °C/min) and (b) during heating (heating rates from the top trace to the bottom trace: 20, 10, 5, 25 °C/min).

a Mettler hot stage FP-90, while a JEOL (1200 EX II) TEM was used to study ordered morphology on the nanometer scale. Selected area electron diffraction (SAED) experiments were also carried out using TEM (the accelerating voltage was 120 kV). The TEM samples on carbon-coated glass surfaces were shadowed by Pt for better contrast. The samples were then detached from the glass surface and picked up on the Cu grids. Calibration of the ED spacing was conducted by using TlCl and Au.

An AFM (Digital Instrument Nanoscope IIIa) was used to examine the surface topology of the C_{14}PhBA thin film treated as described before. A 100-μm scanner was selected, and the contact mode was used to obtain both height and phase images. The force used by the cantilever was light enough to limit damage to the sample, yet sufficient so that the surface features could be accurately explored. The scanning rate was controlled to be 1−3 Hz for the low-magnification images. The data were collected with a 512 × 512 pixels per image resolution.

To study the surface topology of the self-assembled structure in the thin films, the polyethylene (PE) surface lamellar decoration (SLD) technique[24,25] was applied to investigate the supra-molecular packing. In brief, a linear PE was used as the decoration material (M_n = 17.3k g/mol and polydispersity = 1.11, provided by Phillips Petroleum Co.). The decoration was conducted in a vacuum evaporator. The PE was degraded, evaporated, and deposited onto the self-assembled column surface.

Crystallographic simulation was performed using a Cerius 2 software with COMPASS force field. To make the simulation practical, tetradecyl tails were replaced by methyl groups. The conformation of the lowest energy for the molecule was chosen as the starting conformation. Crystallographic data from WAXD were used to fix the dimensions of the unit cell during energy minimization.

Results and Discussions

Thermal Properties of Phase Transformations. Parts (a) and (b) of Figure 1 show two sets of DSC heating and cooling diagrams for C_{14}PhBA at rates ranging between 2.5 and 20 °C/min. At a cooling rate of 2.5 °C/min, two major transition processes are observed at 146 and 52 °C, respectively. The heat of the high-temperature transition is 40.5 kJ/mol, while that of the low-temperature transition is 54.7 kJ/mol. These heats are independent of the cooling rates. At a 2.5 °C/min heating rate, the low- and high-transition temperatures are at 58 and 150 °C, respectively, and possess the identical heats of transition as those measured during cooling. Furthermore, these transition temperatures and heats of transitions are independent of cooling and heating rates. It is noted that tetradecane crystals show a heat of transition between 35 and 40 kJ/mol. In C_{14}PhBA, we have six tetradecyl tails in each molecule. If all of these tails were crystallized, the heat of transition has to be about 4−5 times greater than this value. Therefore, we speculate that the tetradecyl tails in C_{14}PhBAs are not crystallized, and rather, there may remain some mesomorphic order in these tails at low temperatures (see below).

Although DSC experiments are sensitive to heat absorption and release, this technique does not provide information about structure or molecular interactions. We need to utilize spectroscopic and WAXD experiments to identify the interactions and phase structures in C_{14}PhBA.

Molecular Origins of the Phase Transformations. To understand the molecular nature of these phase transformations, FT-IR, Raman, and ^{13}C solid-state NMR spectroscopic techniques were carried out. Figure 2a presents a set of FT-IR spectra of C_{14}PhBA at different temperatures. At room temperature, the rigid amide core exhibits the characteristic bands of aromatic rings at 1608, 1582, 1527, and 1493 cm^{-1} and amide groups at 3300 cm^{-1} (ν_{N-H}, ν: stretching vibration), 1648 cm^{-1} (amide I, $\nu_{C=O}$ makes major contribution), 1550 cm^{-1} (amide II, $\delta_{N-H}+\nu_{C-N}$, δ: scissoring mode), and 1235 cm^{-1} (amide III, $\nu_{C-N}+\delta_{N-H}$). The bands attributed to the aliphatic tails can be found at 2957 cm^{-1} ($\nu_{as}(CH_3)$, asymmetric stretching), 2921 cm^{-1} ($\nu_{as}(CH_2)$), 2873 cm^{-1} ($\nu_s(CH_3)$, symmetric stretching), 2851 cm^{-1} ($\nu_s(CH_2)$), 1468 cm^{-1} ($\delta(CH_2)$), 1382 cm^{-1} (CH_3 umbrella), and 720 cm^{-1} ($(CH_2)_n$ rocking, $n \geq 4$). Frequency, intensity, and shape of IR absorption bands can be correlated with conformations and/or molecular interactions. As one of the strongest physical interactions, H-bonding can impose prominent influence on the involved IR bands. The ν_{N-H} and amide I bands are known to be sensitive to H-bonding. The observed ν_{N-H} (3300 cm^{-1}) and amide I (1648 cm^{-1}) clearly indicate that at room temperature almost all the N−H groups in C_{14}PhBA are associated with the C═O groups via N−H···O═C H-bonds. This is supported by the fact that "free" (non H-bonded) N−H stretching bands (a relatively sharp peak with a frequency higher than 3400 cm^{-1}) are not observed.[26,27] This is further supported by the fact that the ν_{N-H} band becomes weaker and shifted toward higher frequencies upon heating, which is typical for H-bonded N−Hs. This phenomenon of no "free" N−H bands can be observed up to the immediate

(24) Wittmann, J. C.; Lotz, B. *J. Polym. Sci., Polym. Phys. Ed.* **1985**, *23*, 205−226.
(25) Chen, J.; Cheng, S. Z. D.; Wu, S. S.; Lotz, B.; Wittmann, J. C. *J. Polym. Sci., Polym. Phys. Ed.* **1995**, *33*, 1851−1855.
(26) Skrovanek, D. J.; Howe, S. E.; Painter, P. C.; Coleman, M. M. *Macromolecules* **1985**, *18*, 1676−1683.
(27) Harris, P. I.; Chapman, D. *Biopolymers (Peptide Sci.)* **1995**, *37*, 251−263.

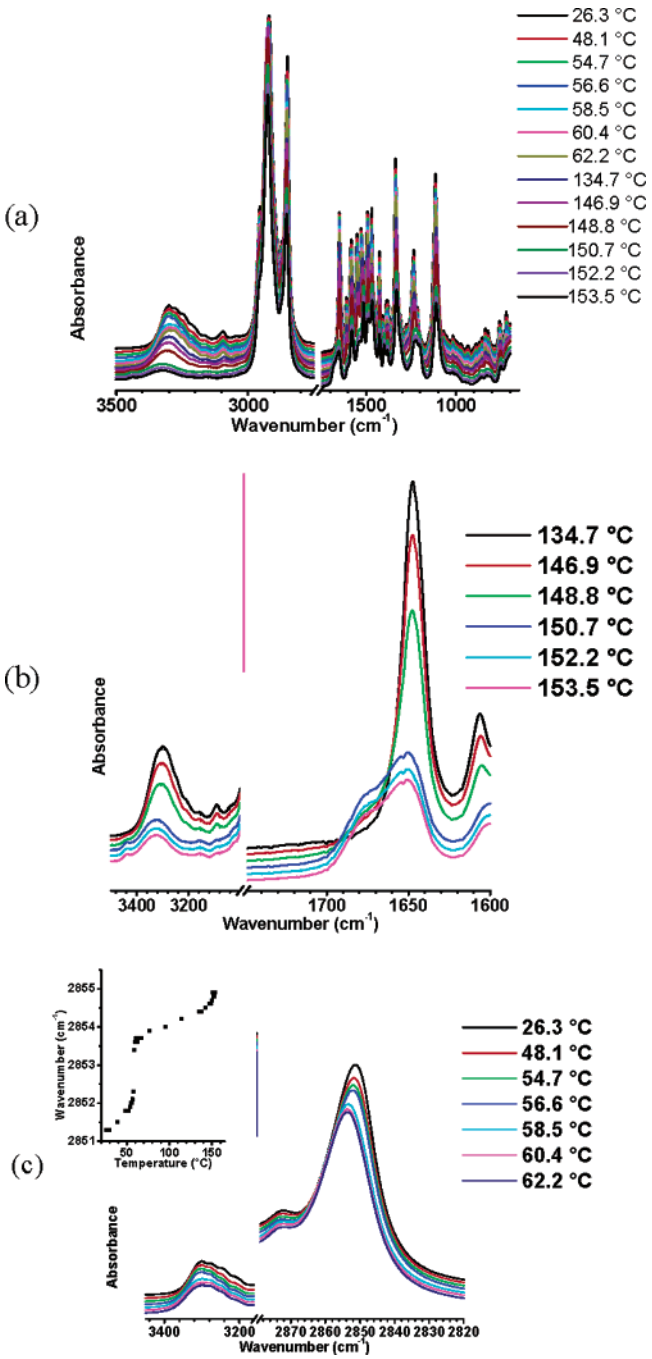

Figure 2. FT-IR spectra during heating: (a) 3500−2750 and 1750−700 cm^{-1} regions, from room temperature to 153.5 °C; (b) 3500−3000 and 1750−1600 cm^{-1} regions between 134.7 and 153.5 °C; (c) 3450−3160 and 2880−2820 cm^{-1} regions from room temperature to 62.2 °C. The inset in Figure 2c shows how the frequency of $\nu_s(CH_2)$ changes with temperature.

vicinity of the isotropization temperature. Above this temperature, a weak, relatively sharp absorption band at 3441 cm^{-1} attributed to the "free" N−H stretching vibration appears. This is accompanied by a sudden blue shift and an abrupt drop in intensity of the H-bonded ν_{N-H} originally at 3300 cm^{-1}. At the same time in the amide I region, the "free" stretching band appears as a shoulder at 1680 cm^{-1} at the expense of the H-bonded band (1648 cm^{-1}) as shown in Figure 2b. A careful examination of the FT-IR spectra found that the ν_{N-H} band also changes discontinuously at the low-temperature transition, but with a much smaller amplitude as

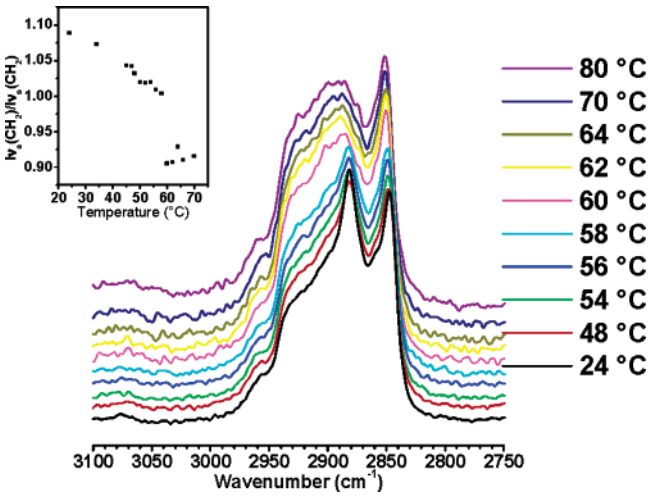

Figure 3. C−H stretching region of Raman spectra, from room temperature to 80 °C. The I_{2847}/I_{2881}−temperature plot is shown as the inset.

depicted in Figure 2c. On the basis of these observations, it can be concluded that nearly 100% of the N−H and C═O groups are linked by H-bonds at room temperature. Although they gradually become weaker with increasing temperature, these H-bonds remain in the entire temperature range until reaching the isotropization temperature. Significant dissociation of H-bonds only takes place above the isotropization temperature.

While the ν_{N-H} and amide I can be correlated with H-bonding, the $\nu_{as}(CH_2)$ and $\nu_s(CH_2)$ are utilized to probe alkyl chain conformations. It is known that, for an all trans alkyl chain, the $\nu_{as}(CH_2)$ and $\nu_s(CH_2)$ are typically in the ranges of 2846−2850 and 2916−2920 cm^{-1}, respectively. For disordered alkyl chains, as in liquid *n*-alkanes, these ranges shift to 2854−2856 and 2924−2928 cm^{-1}.[28−30] For C_{14}PhBA at room temperature, the $\nu_{as}(CH_2)$ and $\nu_s(CH_2)$ appear at 2851 and 2921 cm^{-1}, indicating a significant population of the trans conformation. The gauche conformations also exist, supported by the absence of equally spaced CH_2 wagging-twisting progression bands between 1170 and 1350 cm^{-1}, which is characteristic for an alkyl chain with the all trans conformation.[30,31] When the temperature is being increased to below the low-transition temperature of 58 °C, the concentration of gauche conformations continuously increases, as illustrated by the increase of the $\nu_s(CH_2)$ frequency in Figure 2c. However, this frequency increase is discontinuous at 58 °C, indicating an abrupt increase in the concentration of the gauche conformations. As the temperature is further increased, the $\nu_s(CH_2)$ frequency continuously but less significantly increases. Another sudden change at the isotropization temperature is almost not experimentally observable.

The sudden change in alkyl tail conformations at 58 °C is also supported by Raman spectroscopy as shown in Figure 3 with the CH_2 stretching region at varying temperatures. The spectrum at room temperature re-

(28) Snyder, R. G.; Strauss, H. L.; Elliger, C. A. *J. Phys. Chem.* **1982**, *86*, 5145−5150.
(29) MacPhail, R. A.; Strauss, H. L.; Snyder, R. G.; Elliger, C. A. *J. Phys. Chem.* **1984**, *88*, 334−341.
(30) Venkataraman, N. V.; Vasudevan, S. *J. Phys. Chem. B* **2001**, *105*, 1805−1812.
(31) Synder, R. G.; Schachtschnelder, J. H. *Spectrochim. Acta* **1963**, *19*, 117−168.

sembles that of hexagonal phase of n-$C_{36}H_{74}$[32] and that of polyethylene with low crystallinity,[33] but with broader $\nu_{as}(CH_2)$ and $\nu_s(CH_2)$ peaks at 2847 and 2881 cm^{-1}, respectively. The peak intensity ratio of the $I[\nu_{as}(CH_2)]/I[\nu_s(CH_2)]$ (here it is I_{2847}/I_{2881}) has been widely used to probe conformational order of polymethylene chains.[32,34,35] This ratio varies from 2.2 for the chains with the all trans conformation in a crystal to 0.7 for disordered chains in an isotropic liquid.[32] In C_{14}PhBA, this ratio is 1.09 at room temperature, which suggests that the alkyl chains are in a mesophase ordered form with the presence of gauche conformations. The ratio gradually decreases with increasing temperatures until 58 °C, where it suddenly drops to 0.9, as shown by the inset of Figure 3. At the same time, abrupt frequency shifts of the $\nu_{as}(CH_2)$ and $\nu_s(CH_2)$ are also observed, as well as the broadening of the $\nu_{as}(CH_2)$. After this transition temperature, the changes in the spectra are much less prominent. The discontinuous changes in the relative intensities, the shape, and the position of absorption bands at 58 °C suggest a discontinuous increase of the quantity of gauche conformations in the alkyl chains when the low-temperature transition takes place, and this agrees with the FT-IR results.

^{13}C solid-state NMR has the unique advantage of offering a quantitative estimation of the population of the carbon atoms in the long trans segments. For PE chains having the all trans conformation, the ^{13}C chemical shifts of the methylene carbons appear between 33 and 35 ppm, depending on the type of structure. On the other hand, in the I state, random coils, having statistically distributed trans and gauche conformations, resonate from 29.5 to 31 ppm.[36−38] Figure 4 shows the Bloch decay spectra of the C_{14}PhBA at different temperatures. At room temperature, the resonance peak at 33.5 ppm represents those methylene carbon atoms in the long trans zigzag segments in the alkyl tails, while the peak at 30.5 ppm corresponds to the carbon atoms in the disordered, statistically distributed trans and gauche conformations. The population of CH_2 carbons in the long trans segments can be calculated from the relative areas of these two peaks. At room temperature, 64% of CH_2 carbon atoms are in the relatively long trans zigzag segments. When the temperature increases, the intensity of the chemical shift resonated at 33.5 ppm slightly decreases while the intensity of the chemical shift resonated at 30.5 ppm increases accordingly. Between 57.5 and 60 °C, a sudden intensity change can be observed, indicating a phase transition involving the abrupt conformation change in the alkyl tails. At this transition, a majority of the long trans segments are transformed into a liquidlike, disordered state. This is evidenced by the significantly increased intensity of the 30.5 ppm resonance peak as well as the much reduced intensity of the 33.5 ppm peak. Little change is observed at higher temperatures up to 167.5 °C, after which the liquidlike conformation was reached.

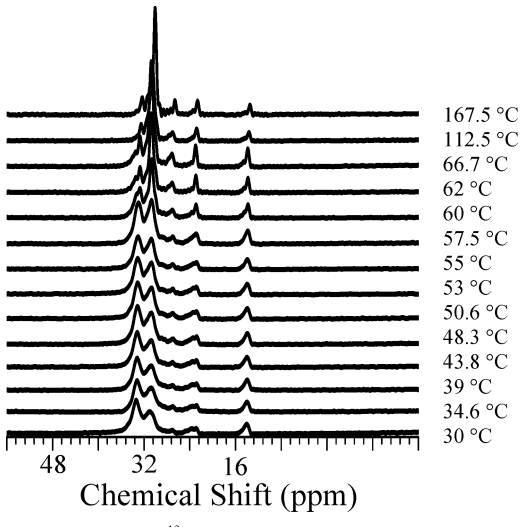

Figure 4. Set of ^{13}C solid-state NMR Bloch decay spectra of the C_{14}PhBA bisamides at different temperatures.

Combining spectroscopy and thermal analysis results, we are in a position to provide a phase structure of C_{14}-PhBA on a molecular length scale in the temperature region up to the isotropization temperature. At room temperature, all the N−H and C═O groups are associated via H-bonds and the alkyl tails are in a mesophase ordered conformation (64% carbon in the long trans segments). The general trend is that H-bonds between rigid amide cores continuously weaken, while more gauche conformations are induced in the alkyl tails with increasing temperatures. A discontinuous alkyl chain conformation change is detected at 58 °C, while the change at the high-temperature transition is much less prominent. This suggests that the low-temperature phase transition is mainly attributed to the discontinuous change in the alkyl tail conformation. On the other hand, the dissociation/weakening of the H-bonds makes the major contribution to the high-temperature phase transition.

"Supra-molecular" Structural Determinations. Ordered phase structures must be determined on the basis of 1D and 2D WAXD experimental observations. Figure 5 shows a set of 1D WAXD patterns scanned while cooling with a rate of 1.0 °C/min from 160 °C to room temperature. At 160 °C, which is above the isotropization temperature, two amorphous halos can be seen in the I phase. The high-angle scattering halo at $2\theta = 18.5°$ (d-spacing of 0.48 nm) is attributed to the average lateral distance among alkyl chains. On the other hand, the low-angle scattering halo at $2\theta = 3.10°$ (d-spacing of 2.85 nm) may represent the average periodicity of electron density fluctuations among the supra-structures caused by a micro-phase separation between the amide cores and alkyl tails (see below). When the sample reaches 146 °C, three overlapped reflections (see below for the 2D WAXD results) can be identified at $2\theta = 2.41°$, 2.70°, and 3.17° (their d-spacings are 3.67, 3.27, and 2.79 nm), and the amorphous halo in the wide-angle region shifts slightly to a higher angle of $2\theta = 19°$ (d-spacing of 0.47 nm). With

(32) Snyder, R. G.; Hsu, S. L.; Krimm, S. *Spectrochim. Acta* **1978**, *34A*, 395−406.
(33) Abbale, S.; Zerbi, G.; Wunder, S. L. *J. Phys. Chem.* **1982**, *86*, 3140−3149.
(34) Wallach, D. F. H.; Verma, S. P.; Fookson, J. *Biochim. Biophys. Acta* **1979**, *559*, 153−208.
(35) Casal, H. L.; Cameron, D. G.; Mantsch, H. H. *J. Phys. Chem.* **1985**, *89*, 5557−5565.
(36) Guo, M.; Krichdeldorf, H. R. *Polym. Prepr.* **1997**, *38*, 274−275.
(37) Earl, W. L.; VanderHart, D. L. *Macromolecules* **1979**, *12*, 762−767.
(38) Wang, L.; Liu, J.; Exarhos, G. J.; Flanigan, K. Y., Bordia, R. *J. Phys. Chem. B* **2000**, *104*, 2810−2816.

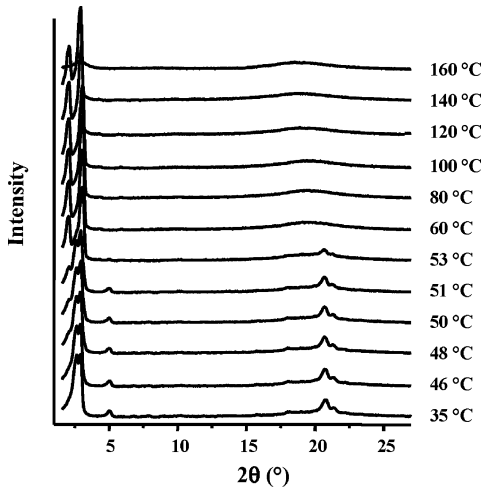

Figure 5. Set of 1D WAXD patterns for C_{14}PhBA during cooling at a rate of 1 °C/min.

further cooling of the sample to 53 °C, the three partially overlapped reflections in the low-angle region change to $2\theta = 2.68°$, 2.88°, and 3.17° (their *d*-spacings are 3.30, 3.07, and 2.79 nm), respectively. In the wide-angle region, the reflections at $2\theta = 20.8°$ and 21.4° start to appear. With further decreasing temperatures, the intensity of the lowest angle reflection is substantially reduced, while the intensities of the reflections in the high-angle region at $2\theta = 20.8°$ and 21.4° are enhanced, indicating an introduction of certain types of order on the sub-nanometer scale. Meanwhile, a reflection at $2\theta = 5.39°$ (the *d* spacing of 1.64 nm) appears and increases its intensity with decreasing temperature. During heating at 1.0 °C/min, the 1D WAXD patterns of C_{14}PhBA are reversible as observed during cooling in Figure 5.

The 2D WAXD pattern of an oriented C_{14}PhBA sample (mechanically sheared) for the low−temperature phase is shown in Figure 6a. On the equator, the overlapped sharp arcs in the low-angle region ($2_\theta = 1.5$−3.5°) can be deconvoluted (Figure 6b). They are attributed to three diffraction spots at $2\theta = 2.68°$, 2.88°, and 3.17°, which agree with those in the 1D WAXD observations (Figure 5), and they are assigned as the (010), (110), and (100) diffractions, respectively. There are also a series of relatively weak diffractions on the equator as shown in Figure 6b. Weak and diffuse diffractions can also be found on the first layer of the 2D WAXD pattern, and they appear as streaks (see below). On the meridian, a relatively diffuse diffraction arc was assigned as the (002) reflections, and its *d* spacing is 0.48 nm. This indicates that the structure along the meridian direction may have a quasi-long-range order. Furthermore, two arcs in the quadrants and on the equator are at $2\theta = 20.8°$ and 21.4°, respectively, which may be assigned to the interchain packing of the mesomorphic ordered alkyl tails based on the spectroscopic results. If we exclude those two diffraction arcs that are attributed to the alkyl tails, a quasi-3D monoclinic cell can be constructed with $a = 3.28$ nm, $b = 3.87$ nm, $c = 0.97$ nm, $\alpha = \beta = 90°$, and $\gamma = 58.1°$ via refinements of the reciprocal lattice using a standard procedure, and this is abbreviated as the Φ_{OK} phase. The *d* spacings of the observed equator diffractions are listed in Table 1. The calculated data are also listed in this table, which were generated using the determined monoclinic lattice parameters. Note that this is close to a hexagonal structure. All the relatively weak diffractions on the equator can be assigned based on these structural parameters as shown in Figure 6b.

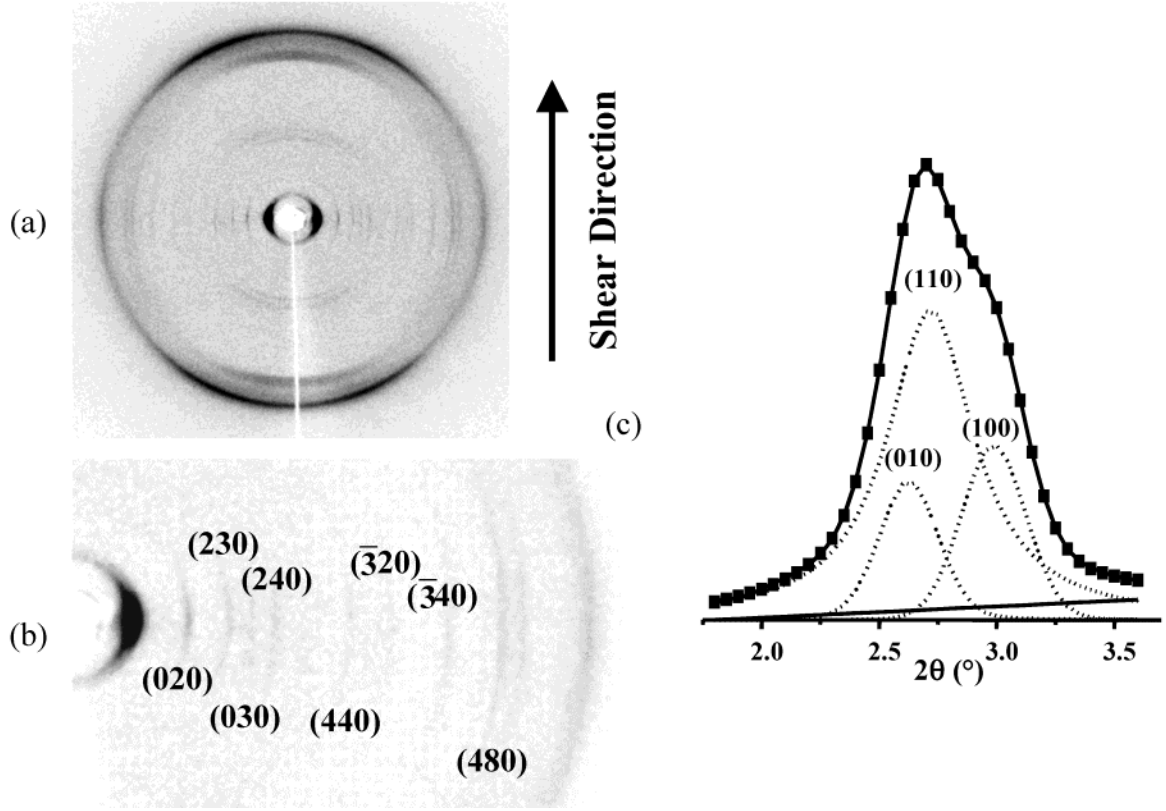

Figure 6. 2D WAXD pattern of mechanically sheared C_{14}PhBA at room temperature (a); the equator diffractions in the low-angle region (b); and the deconvolution of the strongest diffractions below $2\theta = 3.5°$ (c).

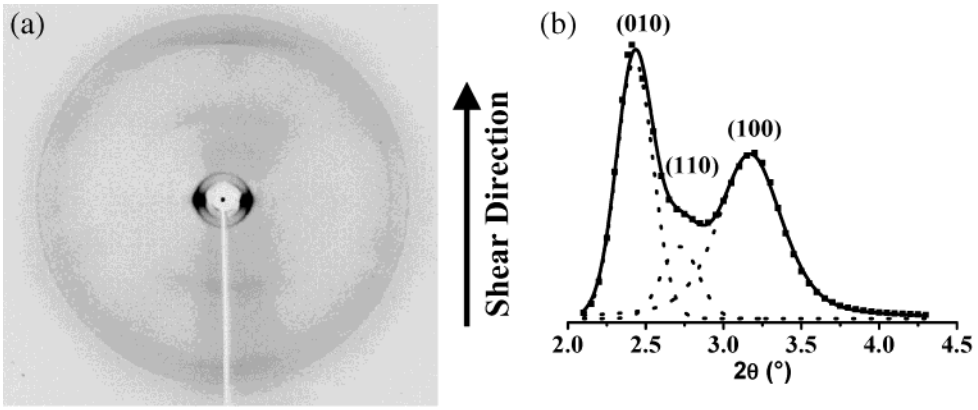

Figure 7. 2D WAXD pattern of mechanically sheared C_{14}PhBA at 120 °C (a); and the deconvolutions of these three equatorial diffractions below $2\theta = 4°$ (b).

Table 1. Observed and Calculated *d* spacings in the Φ_{OK} phase at room temperature

hkl	(100)	(010)	(110)	(020)	(230)	(030)	(240)	(440)	($\bar{3}$20)	($\bar{3}$40)	(480)
obs (nm)	2.79	3.29	3.07	1.64	1.23	1.10	0.96	0.77	0.67	0.50	0.48
calc (nm)	2.785	3.286	3.070	1.643	1.234	1.095	0.965	0.768	0.671	0.498	0.482

The calculated density is 1.00 g/cm^3 if four C_{14}PhBA molecules are in one cell. This is consistent with the measured density of 0.99 g/cm^3.

Figure 7a shows a 2D WAXD pattern of the sheared C_{14}PhBA in the high-temperature phase at 120 °C. On the equator, three overlapped diffraction arcs in the low-angle region at $2\theta = 2.43°$, 2.72°, and 3.17° (d-spacing of 3.63, 3.24, and 2.79 nm) can be assigned as the (010), (110), and (100) diffractions, respectively, based on deconvolutions of the equatorial integration in the low-angle region as shown in Figure 7b. However, those higher order equator weak diffractions that appeared in the low-temperature phase diminished. The two wide-angle arcs near $2\theta \sim 21°$ in the quadrants also no longer exist. This supports our assignment that the $2\theta \sim 21°$ arcs are attributed to the packing of the mesomorphic ordered alkyl tails and agrees well with the spectroscopic data, which suggest that the alkyl tails are liquidlike in the high-temperature phase. The high-temperature "supra-molecular" structure can be identified as a 2D columnar phase (Φ_{OB}) lattice having $a =$ 3.34 nm, $b = 4.62$ nm, $\alpha = \beta = 90°$, and $\gamma = 56.6°$. Again, this 2D structure is close to a hexagonal lateral packing.

Morphology and Molecular Orientation of the "Supra-molecular" Phases. Figure 8a shows the morphologies of the Φ_{OB} phase observed in PLM. When a film sample is isothermally annealed at 145 °C, which is 1 °C lower than the transition temperature of the $\Phi_{OB} \leftrightarrow$ I phases, ribbonlike morphologies are observed with a typical width of a few micrometers. Some of them are folded back and forth while others even form circles, similar to many small LC molecules having cholesteric and highly ordered smectic phases.[39] This is surprising since C_{14}PhBA only exhibits a "supra-molecular" LC phase, and these morphologies must be achieved by self-assembly via intermolecular interactions. It is speculated that the elongated ribbon axis may represent the long axis of the columns. However, the limited resolution of the PLM observations cannot verify this speculation. Heating this sample to 148 °C, which is only 3 °C higher than that shown in Figure 8a, the sample becomes totally dark, indicating a transformation to the I state.

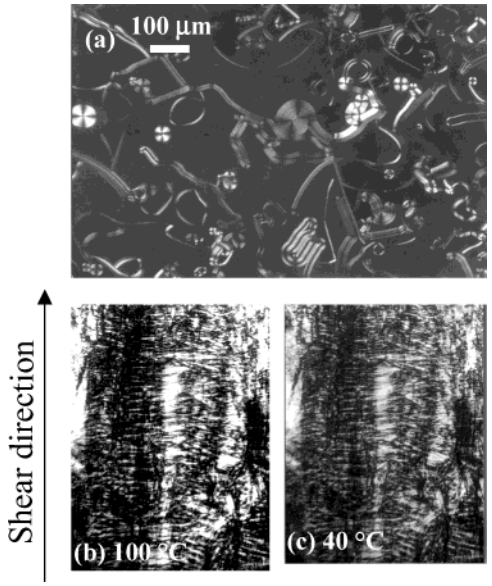

Figure 8. PLM micrograph of the supra-molecular phase morphologies of C_{14}PhBA taken at 145 °C (a); the banded textures of a sheared C_{14}PhBA sample observed at 100 °C in the low ordered phase (b) and 40 °C in the highly ordered phase (c).

When the film samples were sheared by a mechanical force at the temperature of 165 °C and then cooled to 100 °C in the Φ_{OB} phase, a banded texture with a spacing distance of a few micrometers was observed as seen in Figure 8b. The band director is perpendicular to the shear direction. With further decreasing of the temperature to the Φ_{OK} phase at 40 °C, this banded texture remains (Figure 8c). This texture usually appears for LC polymer fluids after some relaxation of the main chain occurs.[40] It is interesting that in these "supra-molecular" phases the self-assembled columns

(39) Demus, D.; Richter, L. *Texture of Liquid Crystals*; Verlag Chemie: New York, 1978.

(40) Ge, J. J.; Zhang, J. Z.; Zhou, W.; Jin, S.; Li, C. Y.; Wang, S.-Y.; Harris, F. W.; Cheng, S. Z. D. *J. Mater. Sci.* **2000**, *35*, 5215−5223.

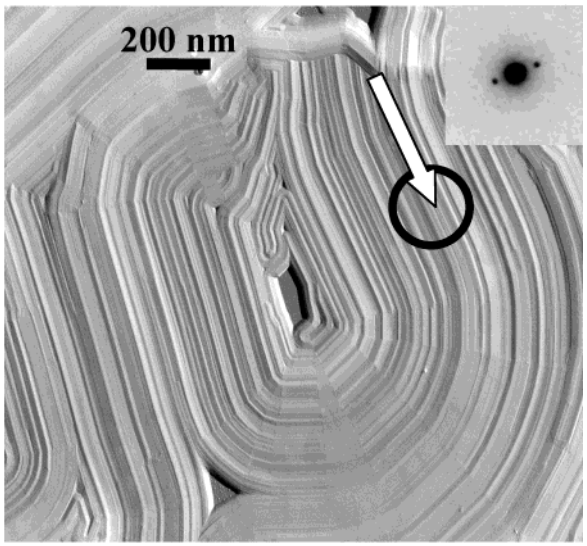

Figure 9. TEM morphological microphotograph with an arrow pointing along the long axis of the columns (the *c**-direction); a selected area electron diffraction pattern from the circled area is shown as the inset.

behave as individual rods in responding to the mechanical shearing.

The TEM morphology of the sample where the SAED patterns were taken to provide direct evidence of the existence of columns is shown in Figure 9. Since the TEM was operated at room temperature, the sample was in the Φ_{OK} phase. The column direction is parallel to the surface of the substrate and highly oriented (indicated by an arrow in Figure 9), which is confirmed by the SAED pattern shown in the inset. There are many edges along the column's long axis, and each edge is around 3−4 nm, which corresponds to the *d*-spacings of the low-angle diffractions in the WAXD observations. Furthermore, AFM provides direct observation of the column's existence. Figure 10a shows a height image of the surface topology of a C_{14}PhBA thin film on a carbon-coated substrate. In this figure, the columns align on the substrate surface with a diameter of about 3.5 nm (see also the height profile in Figure 10b), which is close to the *d*-spacing of the [100] zone (3.3 nm) from the structure determination of the WAXD results.

Moreover, the PE SLD results in Figure 11 show the PE crystal rods are perpendicular to the column's long axis, indicating that the chain axis of the PE oligomers (with a length of ∼20 nm and, thus, the width of the PE rod crystals) are deposited on the edges between the columns, and the PE chains are along the column long axis.[41]

The remaining question is how C_{14}PhBA molecules, which do not have a discotic-geometrical shape, construct columns as building blocks? We first need to know the molecular orientation of this supra-molecular lattice. Figure 12 shows the polarized FT-IR spectroscopy results of the oriented samples prepared by mechanical shearing. With rotation of the polarizing angle from 0° to 90°, that is, the polarization direction of the beam is changed from parallel (0°) to perpendicular (90°) to the shear direction, the H-bonded stretching vibration band

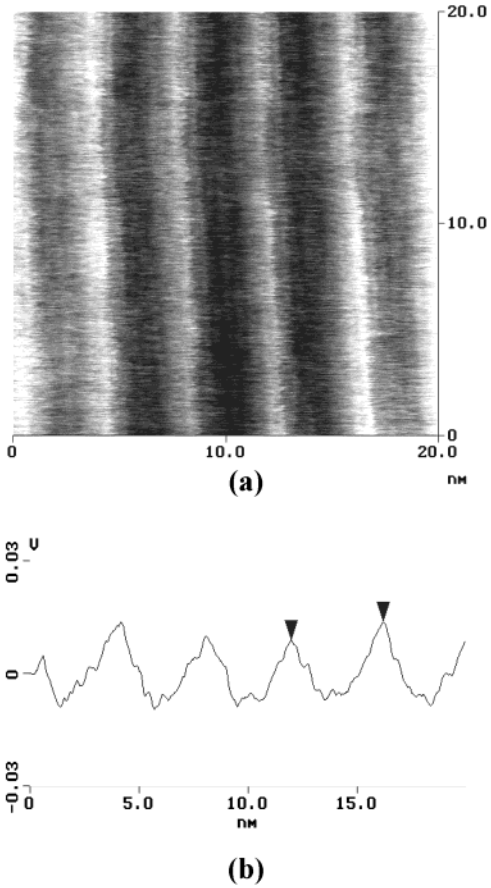

Figure 10. Surface topology of C_{14}PhBA observed in AFM: (a) height image and (b) height profile.

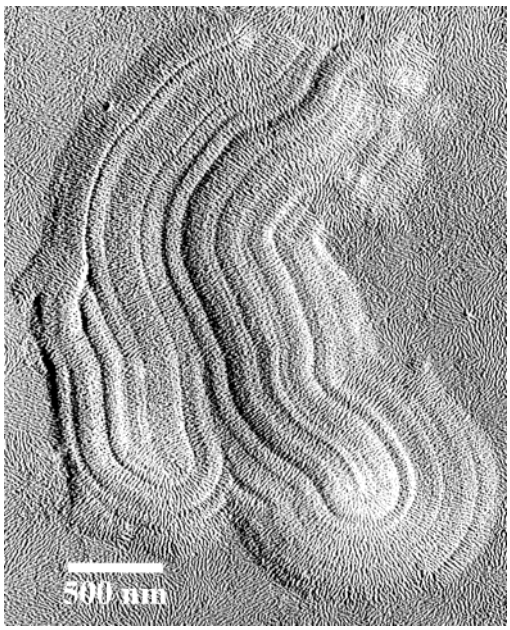

Figure 11. TEM morphology of the self-assembled columns after PE SLD.

of N−H at 3300 cm^{-1} exhibits a decrease in intensity. The dichroic ratio ($A_{//}/A_{\perp}$) of the N−H stretching vibrations is 5.2. Similarly, the dichroic ratio of the amide I band was 5.6. These bands thus exhibit a parallel dichroism, indicating that the transition moments of these stretching vibrations orient preferably along the long axis of the columns. In other words, the N−H and

(41) Ge, J. J.; Li, C. Y.; Xue, G.; Mann, I. K.; Zhang, D.; Wang, S.-Y.; Harris, F. W.; Cheng, S. Z. D.; Hong, S.-C.; Zhang, X.; Shen, Y. R. *J. Am. Chem. Soc.* **2001**, *123*, 5768−5776.

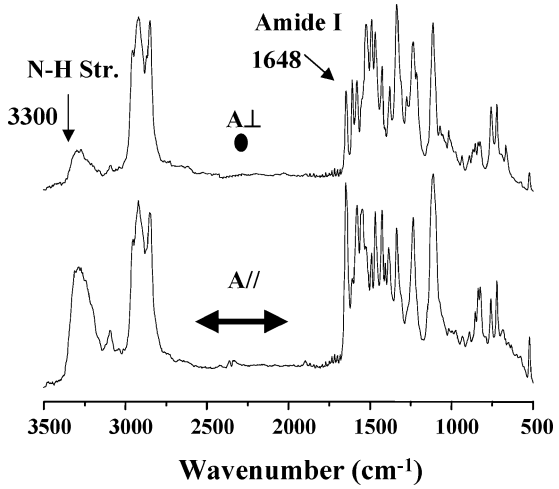

Figure 12. Polarized FTIR spectra of oriented C_{14}PhBA with radiation polarized parallel ($A_{//}$) and perpendicular ($A_{\perp}$) to the direction of the column.

C═O groups prefer to align along the column axis direction. This is confirmed by the perpendicular amide II band, which consists largely of the in-plane N−H bending and C−N stretching having a transition moment nearly perpendicular to that of amide I. Therefore, in an oriented C_{14}PhBA column the long axis of the rigid bisamide core must be approximately perpendicular to the column axis so that they can be connected by the N−H···O═C H-bonds along the column axis.

How the Molecules Self-assemble into the Ordered Supra-molecular Structure. A reasonable packing scheme has to meet the requirements of the unit cell determined using the WAXD structural analysis, the H-bond orientation based on the polarized FT-IR results, and density data. The starting model is shown in Figure 13. Figure 13a is viewed along the long axis of the column, and Figure 13b is along a direction which is perpendicular to the long axis of the column. In this model, the two amide cores of two molecules are face-to-face in an edge-on parallel position (the face-to-face distance between two edge-on amide cores within one pair is ∼0.7 nm), and therefore, the phenylene planes are parallel to the long axis of the column. The neighboring two C_{14}PhBA pairs: one on the top and another on the bottom are rotated 90° along the long axis of the column with respect to each other. The neighboring edge-on amide core pairs along the long axis of the column is ∼0.49 nm, which is appropriate to build up an intermolecular H-bonding between the C═O and H−N groups. As a result, four H-bonds are built up in the neighboring two pairs along the column, and the transition dipole moments of the N−H and C═O stretching vibrations are parallel to the column axis. This alternating 90°-rotation of the amide core pair orientation from one layer to another generates the central frame of a column. The outside peripheral regions are covered by the alkyl tails to form the columns, and these columns are closely packed to construct "supra-molecular" Φ phases on the nanometer length scale.

To test the validity of this model, a unit cell was constructed using the bisamide cores with methyl groups instead of the long alkyl tails. This is because if we used six full alkyl tails, the model would have too many atoms to practically perform the simulation. A methyl group provides a similar steric hindrance at the immediate vicinity of the bisamide cores, and therefore, the local environment of rigid cores is kept close to the real system. A problem has, however, appeared with this treatment; namely, the electron density contrast in all directions except the direction along the column long axis will be artificially enhanced. This is because we are using the experimentally determined unit cell parameters, which means that a vacuum effectively replaces alkyl chains at the outer boundary of the aromatic cores. Nevertheless, as the cores possess considerably higher electron density than the tails, the main feature of the real electron density profile will not be distorted too much by replacing the low-electron-density alkyl chains with vacuum to provide a qualitative illustration. Figure 13c shows a simulated 2D WAXD fiber pattern generated using the proposed model. The vertical position of each column along the column axis is adjusted randomly to simulate the packing in the 2D laterally ordered columnar phase using a 3D-ordered simulated crystalline structure. The generated diffraction pattern is not

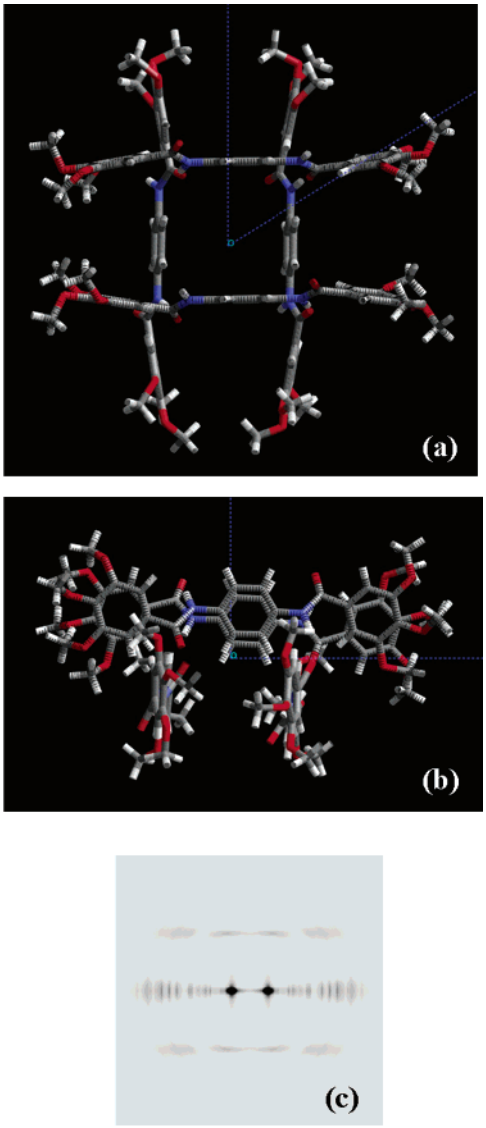

Figure 13. Starting molecular packing model in the supra-molecular structure based on WAXD and polarized FT-IR results: the top view along the column axis (a); the side view (b); the simulated fiber diffraction pattern (c). The upper bisamide pair was shadowed.

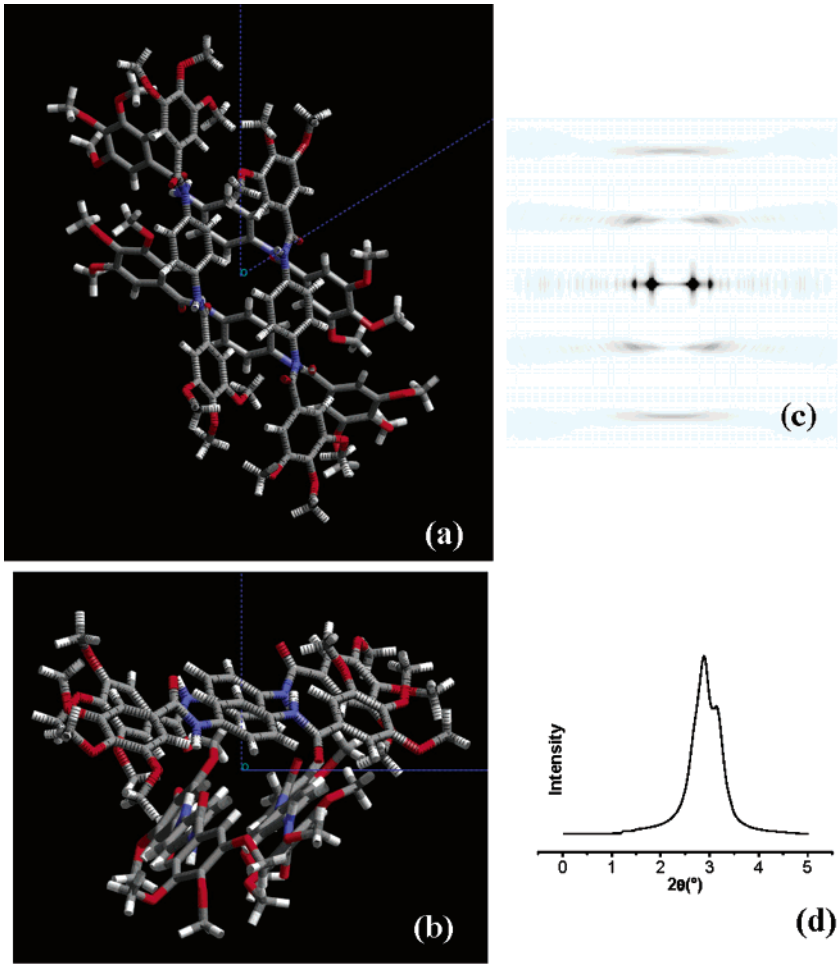

Figure 14. Energy-minimized model with the top view along the column axis (a); the side view (b); the simulated fiber diffraction pattern (c); and the equatorial scan of the simulated fiber pattern (d). The upper bisamide pair was shadowed.

even close to the observed one. Furthermore, an energy calculation shows that this model is energetically unfavorable. One major factor that destabilizes the system is that there is considerable empty space at the center of a column. An energy minimization with the fixed unit cell dimension gave rise to a model with a much lower energy (1387 kJ/mol lower), which is shown in Figure 14a,b. In this model, there are still four H-bonds between two neighboring pairs running along the column direction, but the phenylene rings of the bisamide cores are tilted with respect to the column axis, and phenylene rings of two amide cores in the pair are in a distorted face-to-face configuration. As a consequence, there is less empty space at the center of a column. To have this energy-favorable arrangement while still keeping four H-bonds between two neighboring bisamide pairs, the angle between two adjacent bisamide pairs along the column direction becomes 50°.

The simulated 2D diffraction after using the energy-minimized model is shown in Figure 14c. This pattern agrees qualitatively with the experimental observation but without the arc at $2\theta = 20.8°$ in the quadrants and the arc at $2\theta = 21.4°$ on the equator. Again, this suggests that these two arcs are attributed to the ordered alkyl tails since we do not include these alkyl tails in this simulation. On the equator, all the simulated diffractions fit qualitatively with the experimentally observed arcs shown in Figure 6. In the low 2θ angle region, positions and relative intensity ratios of the equatorial reflections also fit with those observed in the experiments (Figure 14d). In the wide-angle region, the weak (002) layer reflections on the meridian can also be seen. In the simulated pattern of Figure 14c, the first layer reflections parallel to the equator appears as streaks, and again, this is close to the experimental observation. Moreover, the intensity distribution along the first layer line qualitatively agrees with the experimental data: the center (on meridian) is significantly weaker than those in quadrants. In the simulated diffraction pattern, however, the second layer is slightly weaker than the first layer, but in the observed pattern the second layer is stronger. This is because, in the model, we have a significant amount of vacuum area between columns, in sharp contrast with the alkyl chains present in reality. This leads to a higher electron density contrast in the direction perpendicular to the column axis. Those diffraction streaks in the first layer benefit from the higher contrast considerably, but the (002) diffraction cannot since it does not involve any intercolumn spacing.

Conclusion

In summary, the structural analysis via WAXD combined with the molecular orientation information determined by polarized FT-IR experiments has provided experimental evidence to determine the H-bonding induced "supra-molecular" columnar structure. The

formation of the self-assembled structure is dictated by the amide cores/alkyl tails micro-phase separation and the H-bonding interactions of the rigid cores. The micro-phase separation ensures the H-bonding formation between the amide rigid cores to form the building blocks (columns), yet the alkyl tails are located at the outside peripheral regions of the columns. They interact with other columns to self-assemble the supra-molecular LC Φ phases. On the basis of the FT-IR, Raman, and ^{13}C solid-state NMR experimental results, the alkyl chains themselves possess a mesophasic order at room temperature. Disordering of the alkyl chains is responsible for the low-temperature phase transition ($\Phi_{OK} \leftrightarrow \Phi_{OB}$), while the dissociation of H-bonds destabilizes the "supra-molecular" Φ_{OB} phase and leads to the I state. By tuning these two interactions via specifically altering the rigid core, the number and length of the alky tails, and the chemical structure of these cores and tails, we may design a series of molecular structures to control not only their supra-molecular structures but also the formation pathway of the self-assembling process for specific bio- and optical applications.

Acknowledgment. This work was supported by the NSF (DMR-0203994) and the Collaborative Center in Polymer Photonics between AFRL Materials and Manufacturing Directorate and The University of Akron.

CM0349755